Anisotropy in Sand-Fibre Composites and Undrained Stress-Strain Implications

Ghadr, S.[1,*], Bahadori, H.[2], Assadi-Langroudi, A[3]

[1*] PhD Graduate, Civil Engineering Department, 15 Km Sero Way, Urmia University, Iran

[*Corresponding Author]

E. soheil.ghadr25@gmail.com

[2] Associate Professor, Civil Engineering Department, 15 Km Sero Way, Urmia University, Iran

[3] Senior Lecturer, Civil Engineering group, University of East London, London, England, UK

E16 2RD, England

E. A.AssadiLangroudi@uel.ac.uk

Abstract: Among the plethora of studies on anisotropy in fibre reinforced sands, there exists conflicting views on effects on the steady-state deformations of initial packing. These conflicting views are further confused by strictly limited experimental evidence on flow in complex loading environments, where the principal stresses rotate whereby shearing and torsional stresses combine, and when extension in soil relives the compressive stresses. In the heuristic of intrinsically anisotropic nature of the soil and in recognition of the inability of placement methods to overcome such anisotropy, this paper aims to use the orientation if principal stress and soil initial packing state combined as proxy parameters to further the knowledge of plastic behaviour in fibre-reinforced sands. This study furthers the knowledge of the dependency of steady states on anisotropy in composite geomaterials. In doing so, the direction of principal stress orientation is varied from 15° to 60° (from vertical axis), taking an intermediate principal stress ratio of 0.5 and 1.0 and two initial confining pressures. Twenty-four undrained torsional shear tests are conducted using a Hollow Cylindrical Torsional shear Apparatus (HCTA). Under compression and plain strain conditions, torsional stresses limit the improvements in soils' undrained shear strength upon fibre reinforcement. Extension in soil remarkably increase fibres' contribution to betterment of undrained strength. Fibres

are least effective under low isotropic confining pressures and also for certain ranges of torsional stresses.

Keywords: Anisotropy, fibre, reinforced, sand, shear strength, stress path, torsion

1. Introduction

Undrained stressing of sand can pose a number of geotechnical complications, mostly in form of liquefaction [1-4] and flow upon static or monotonic loading [5]. Static loading has a significant role in commencement of liquefaction as well as post-liquefaction flow slide [6-7]. Use of short thin fibres in sand to relax the flow complications is fairly well established; The technique however has never been fully adopted in ground engineering practice. Placement of discrete thin inclusions (e.g. fibre) into sand can enhance soil's tensile strength. Practical examples include reinforced earth transport infrastructure embankments and offshore turbine foundations [8]. Inclusions generally work in tension and improve the shear strength of composite soils they lay in. The stressing response of composites however is complicated and in mediums with rotating principal stresses has remained a matter of dispute.

Sand is a stratified earth material of, by-and-large, inherent anisotropic properties. Stress-strain behaviour of sand depends on orientation of principal stresses with reference to the depositional plane. Placement of fibres in sand can generate higher degrees of anisotropy and further confuses the analysis of flow failure.

Fibres in soil have a close interdependent relationship with soil particles' packing state, shape and form, as well as fibres' spatial arrangement (distribution, orientation, and packing). The implications of fibres' arrangement in soil widely vary. Early studies include the seminal works of Waldron [9] on the effect of plant rootlet systems in stabilisation of soil slopes. For a single fibre in soil, Gray and Ohashi [10] and Maher and Gray [11] proposed a suite of soil-fibre interaction models based on statistical theory of strength for composites and discussed the significance of size distribution and shape of sand, and fibre aspect ratio in composites' stress-strain behaviour. Michalowski and Zhao [12] and Michalowski and

Cermák [13] furthered the understanding of soil-fibre composites; they however assumed that fibres distribute evenly in soil and form an isotropic medium. Michalowski [14] contended the idea and showed that conventional groundworks involving in mixing-rolling-compaction yields a disperse laminated structure of preferred orientations, whereby anisotropy increases. More recently, Diambra et al. [15] and Ibraim et al. [16] showed a tendency for non-uniform distribution of fibres in soil when fibres are mixed with wet soil and compacted using conventional field roller plants. Loading and geometrical anisotropy play a key role. Early attempts in geometrical anisotropy drew on findings from direct shear experiments [17-18], and collectively illustrated the fundamental dependency of the strength of fibre-reinforced soils on the fibre orientation. Among early attempts in loading anisotropy, Symes [19] conducted a suite of drained triaxial shear tests on the medium loose sand at $\alpha = 45°$ and b = 0, 0.14, 0.5 and 1.0. They showed that sand reaches maximum strength and stiffness when sheared at close to plain strain conditions (b = 0.3 to 0.5), whilst lowest strength is typically gained at b = 1.0. Sayao and Vaid [20] made similar observations for medium loose Ottawa sand. Recent findings of Li [21], Diambra et al. [22], Ibraim et al. [16] and Mandolini et al. [23] confirm the existence of anisotropy and debate the enhancement of tensile strength upon fibre reinforcement. These findings generally highlight the substantial impact of placement method on packing state and isotropy in reinforced soils. In the heuristic of intrinsically anisotropic nature of the soil and in recognition of the inability of placement methods to overcome such anisotropy, this paper aims to use the orientation of principal stress and soil initial packing state combined as proxy parameters to further the knowledge of plastic behaviour in fibre-reinforced sands.

Throughout the divergent shear test techniques is the Hollow Cylinder Torsional Apparatus (HCTA) that allows an independent control of the magnitude and direction of principal stress axes in conjunction with a measurement of volumetric and pore pressure variations. HCTA facilitates stress path testing by allowing free rotation of principal stress directions (α) and the intermediate principal stress ratio (b), where α is the orientation of the σ_1 axis to the vertical, the ratio b is $(\sigma_2 - \sigma_3)/(\sigma_1 - \sigma_3)$, and $\sigma 1$, σ_2, and σ_3 are the major, intermediate and minor principal stresses, respectively. The stress-strain behaviour

of soil varies with variation in α and b-ratio values. The majority of the previous experimental works with HCTA have made use of reconstituted clay, sand and often sand-clay specimens [19, 24-27]. Many studies have found strong links between soil strength-stiffness and the direction of the major principal stresses, varied in experiments from 0 to 90° [6, 28-29]. A subset of studies has concluded that sand tends to behave softer as α and b increase under undrained conditions [30]. Many studies have referred to the contractive behaviour of sand with an increase in α and b-ratio values [31-35]. Findings are often conflicting and in cases are further confused by strictly limited experimental evidence concerning flow rule for reinforced granular materials (i.e. sand in particular) that defines the plastic mechanisms under rotating principal axes. In particular, a consensus on the implications of initial packing state is yet to be reached. This study offers fresh insights drawn from 24 undrained torsional shear tests on well-sorted angular silica sand in unreinforced and reinforced forms (with 1.5% microsynthetic fibres). In doing so, the direction of principal stress is varied from 15° to 60°, for an intermediate principal stress ratio of 0.5 and 1.0 and varied initial confining pressure.

2. Materials and Methods

2.1 Testing Materials

Sharp, bimodal, moderately well sorted fine Firoozkuh 161 (F161) silica sand is used as base material of testing specimens. F161 sand is predominantly siliceous (SiO_2 > 96%, Fe_2O_3 = 0.2-0.7%, Al_2O_3 = 0.5-1.6%, CaO = 0.2-0.5%, Na_2O = 0.03-0.08%, K_2O = 0.03-0.10%). Fig. 1a illustrates the particle size distribution for F161 sand. Fig. 1b shows the shape and texture of base F161 sand in a scanning electron microscopy image.

Commercially available thermoplastic polymeric micro synthetic fibres (MEX200^{TM}) with a ribbed linear texture (to improve the adhesion with surrounding soil) and wave-shape cross-section (Fig. 2) are adopted as the reinforcement component. MEX200 fibres are commonly used in concrete industry as tension resistant elements (offering 450 MPa tensile resistance). Fibres used in this study are 0.2 mm in equivalent diameter (D_f) and 15 mm in length (l_f), yielding a mean aspect ratio ($AR_F=l_f/D_f$) of 75 that

is consistent with commonly practiced fibre aspect ratio for reinforced systems in groundworks and also previous studies. Typical aspect ratios range between lower-bound 10 to ensure a reasonable interaction between soil and fibre reinforcements [36] and upper-bound 100 [37]. Table 1 summarizes the geometrical, physical and mechanical properties of constituting sand and fibre used in this study.

2.2 Specimen Preparation

Several methods exist for remoulding granular soils sample at laboratory-scale. The base soil can be moist, dry or saturated; it can be placed using dry deposition, water sedimentation, pouring or spooning techniques; and can be compacted by tapping, tamping, or vibration [38-40]. In this work, the hollow cylinder specimens were synthesised through spooning of randomly mixed sand-fibre assemblages, mixed with water to a low 10% moisture content (i.e. higher than hygroscopic moisture content), into moulds. Spooned wet mixtures were then packed by controlled vibration before saturation. Vibration minimises the chance of wet sand deposition in layers and hence formation of unwelcomed weak planes [41], and also allows the initially metastable loose packing to adopt a denser random packing state. The advantage of this method is the ease of its adoption in field conditions.

Measures were put in place to maintain the uniformity of fibre distribution, to limit the unwelcomed effects of segregation of specimens' constituents. Sample preparation followed two phases. In the first phase, base sand and fibres were manually mixed at predetermined mass proportions. Small amounts of fibres were gradually and 'randomly' added to the mix until, by visual examination, even distribution of fibres throughout the soil mass was ensured (Fig. 3). Water content was raised to 10% through spraying distilled deionised water whilst fibres were gradually added to the mix. To ensure the homogeneity, thoroughly mixed combinations of sand-fibre were spooned into the annulus space between the inner membrane (that surrounds the inner mould) and outer membrane (that covers the outer mould from the inner surface) in five layers to minimise segregation of the fibres (consistent with procedures followed in earlier attempts including Ibraim and Fourmont [42]). The adhesion between sand and fibres at low 10% water content is deemed enough to retain the original random packing

during the placement of mix into triaxial mould, although the angularity of sand is broadly believed to induce some degrees of cross-anisotropy. Visual inspection of specimens verified the reasonably uniform structure of sand-fibre mixtures. Specimens were prepared to a height (L) of 120 mm, inner and outer diameters of 120 mm and 200 mm (r_o=100 mm, r_i=60 mm), respectively. The mould was vigorously vibrated (using a tamping rod) in a similar manner practised in Ibraim et al. [16] and Mandolini et al. [23] and was repeatedly weighed up to achieve the desired placement unit weight. Test specimens were jacketed between two membranes, outer and inner, and sandwiched between two Porous discs at the bottom and on the top. Gaseous CO_2 and de-aired water were gently percolated through the bottom drainage and passed upwards through specimens. A 0.96 and above Skempton's B-value was deemed to represent a fully saturated condition. Following saturation, specimens were isotopic consolidated to 200 kPa and 400 kPa confining pressures, roughly, representing typical stress conditions at base of 10 to 20 mm high fills and earth embankments. Adopted confining pressures also allow findings here to be studied in conjunction with previous similar studies. In the majority of previous fibre-reinforced soils studies, test specimens are synthesised to either a desired relative density or void ratio (e.g. Michalowski and Cermak [13]); the latter is adopted here. Void ratio for each test specimen was measured at the end of each triaxial test through measuring specimens' [saturated] water content and specific gravity, considering a unit degree of saturation and using phase relationships. The post-consolidation void ratio, e_c, fell within the range 0.795 to 0.800 for all test specimens. The extremely low standard deviation of e_c (0.0025 to 0.0035) lends evidence to efficiency the adopted remoulding techniques in ensuring the homogeneity across all test specimens. Specimens were sheared under two initial confining pressure values (P'_c - initial effective mean principal stress) of 200 and 400 kPa.

2.3 Testing Apparatus and Methods

Soil behaviour is fundamentally stress path dependent. The stress path for geotechnical structures can appear in form of principal stresses, rotating about three axes. Unlike the conventional triaxial shear apparatus, Hollow Cylinder Torsional Shear (HCTS) apparatus allows simultaneous application of axial

load, torque, internal and external pressures; hence incorporates a control on both principal stress direction and intermediate principal stress into the stress path approach. As such, HCTS offers the chance to simulate soil's inherent anisotropy and study its implications on stress-strain [post-peak] behaviour. Fig. 4 illustrates the HCTS apparatus used together with test specimen during undrained test.

Twenty-four consolidated undrained (CU) shear tests were conducted on reinforced (1.5% fibre content by mass) and unreinforced sand specimens by varying α and b-ratio values. Testing variables include the inclination angle of the maximum principal stress with respect to the depositional direction (α), initial mean effective stress, intermediate principal stress ratio, void ratio after consolidation and fibre content. Table 2 summarizes the testing variables. CU tests were conducted under two values of initial effective confining pressure (i.e. 200 and 400 kPa), at 0.5 and 1.0 intermediate principal stress ratio (b). Findings are presented in form of effective stress path and stress-strain envelopes.

To apply the inner and outer cell pressures, four Electrical/Pneumatic transducers in addition to the axial and torsional loads pneumatic actuators were utilised. In total, eleven transducers were used. To capture the post-peak soil behaviour, a step motor for torsional strain tests was utilised. The rate of the cylinder twist was 0.5 degree/min; which is the lowest possible torque rate offered by the apparatus. The principal stress direction (α) and intermediate principal stress ratio (b) were kept constant throughout the torsional shear tests (Fig. 5). The inner chamber is isolated from the outer confining chamber, allowing the variation of stress at the inner boundary of the test specimen to be completely independent of that of the outer boundary.

The principal stresses are formulated in Equations 1 and 2: σ_1 is the major principal stress (that is rotated in this work to simulate a suite of anisotropic loading scenarios), σ_2 is intermediate principal stress (equal to the radial stress σ_r), and σ_3 is minor principal stress.

$$\sigma_1 = \frac{\sigma_z + \sigma_\theta}{2} + \sqrt{\left(\frac{\sigma_z - \sigma_\theta}{2}\right)^2 + {\tau_{z\theta}}^2} \qquad (1)$$

$$\sigma_3 = \frac{\sigma_z + \sigma_\theta}{2} - \sqrt{\left(\frac{\sigma_z - \sigma_\theta}{2}\right)^2 + {\tau_{z\theta}}^2} \quad (2)$$

In Eq. 1 and 2, σ_θ is the circumferential normal stress, σ_z is the vertical normal stress (i.e. deviator stress), σ_r is the radial normal stress and $\tau_{z\theta}$ is the torsional shear stress that applies to the specimen. Equations 3 to 5 formulate σ_z, σ_r, $\tau_{z\theta}$ [19], where r_i and r_0 are inner and outer radii of the sample and *T* is monotonic torque. σ_z is formulated as a function of circumferential and radial stresses in Equation 6 and 7 [19].

$$\sigma_\theta = \sigma_z - \frac{2\tau_{z\theta}}{tan2\alpha} \quad (3)$$

$$\sigma_r = \sigma_z - \frac{\tau_{z\theta}(Cos2\alpha - 2b + 1)}{sin2\alpha} \quad (4)$$

$$\tau_{z\theta} = \frac{1}{2}\left\{\frac{3T}{2\pi({r_0}^3 - {r_i}^3)} + \frac{T}{\pi({r_0}^2 + {r_i}^2)(r_0 - r_i)}\right\} \quad (5)$$

$$\sigma_z = \frac{F_v + \pi(P_0{r_0}^2 - P_i{r_i}^2) - A_r P_0}{A_s} \quad (6)$$

$$\begin{cases} P_i = \dfrac{\sigma_r(r_0 + r_i) - \sigma_\theta(r_0 - r_i)}{2r_i} \\ P_0 = \dfrac{\sigma_r(r_0 + r_i) - \sigma_\theta(r_0 - r_i)}{2r_\theta} \end{cases} \quad (7)$$

where F_v is the surface tractions-vertical force, and A_r and A_s are cross-section areas for axial rod and the specimen, respectively. HCTS load and stress conditions are graphically illustrated in Fig. 6, and a photograph of a typical specimen before and after testing is shown in Fig. 7.

3. Results and Discussions

3.1 Phase Transformation

The stress-dependent transition in sand, from an initial compressive to dilative state, takes place along a 'phase transformation' line under undrained condition. The location of the phase transformation line is dependent on minor and intermediate principal stresses, so too sand's relative density [43]. On the q-p' space, phase transformation occurs on the effective stress path; when the stress path changes in direction for effective mean normal stress (p') to reaches its minimum (Fig. 8a). Taking 'steady state' as the state of deformation under constant stress components [44-47], the point of phase transformation can be regarded as a 'steady state'; this state is broadly referred to as the quasi steady state (QSS), where post-peak deformations appear under constant effective mean stress p'. The QSS is followed by the ultimate steady state (USS). Unlike dense sands, in loose sands under low confinement levels, the QSS at the point of phase transformation occurs at minimum shear stress (Fig. 8b - also see Yoshimine and Ishihara [46]). A course of strain hardening will normally follow the QSS, unless sand is at reasonably large levels of initial effective confining pressures (or at a very loose state whereby confining pressure turns out to be relatively large), in which case no post-peak hardening develops, and the minimum stress state evolves into the critical steady state (CSS).

3.2 Steady State for Base Sand

The first phase of tests encompassed 12 torsional compression CU experiments on unreinforced (base) loose sand specimens. The deviatoric stress-strain response (t - ε_q) and ($t - p'$) are plotted in Fig. 9, where t is half the deviatoric stress (equivalent to the undrained shear strength, ε_q is half the deviatoric strain, and p' is the initial effective mean principal stress. Figs. 9a to 9l demonstrate the effect on the undrained behaviour of anisotropic loading, for a range of principal stress orientations, two levels of confinement and b-ratios (a measure of difference between minor and intermediate stress and therefore balance between the compression and extension during the shearing of test specimens).

Strain softening and flow (static liquefaction) was found to be limited to α = 60° (for all b-ratio values) and α = 30° for sand consolidated under high confining pressure (i.e. relatively denser state ahead of shearing) and b = 1, indicating a stress condition that encompass torsion and extension (Figs. 9a, c and

g). Flow upon shearing appeared to be most pronounced in sands under low 200 kPa confining pressure and combined torsion extension (α = 60° and b = 1, see Fig. 7a).

Immediate observations suggest that upon anisotropic loading (i.e. increasing principal stress direction), flow begins to appear at deep sequences as α reaches 30° (Fig. 9g); and then extends to sands at shallower depths as α reaches 60°. Flow under the moderate α = 30° is probably underpinned by dilative behaviour of dense sand, which deteriorates upon application of torsional actions. No flow was detected at α = 15°. Base sand demonstrates a non-flow (NF) deformation with strain hardening (HS) throughout undrained shearing towards the USS.

The undrained shear strength (also the Critical Stress Ratio CSR) and Ultimate Steady State (USS) are inversely proportional with b-ratio, with an exception of H400f0-1-60 and H400f0-0.5-60 (Fig. 9c), where the effective stress paths converge to reach a common USS. Sand begins to exhibit a softer response and the pure compressive effort applying on soil moderates as the b-ratio increases from an initial 0 to 1: This is in part due to appearance of tensile stresses in soil, the immediate consequence of which is a degree of stress relief in form of combined compression and extension (Figs. 9a, e, i and 9c, g, j). In conventional geotechnical design, a 0.3 to 0.5 b-ratio generally is indicative of plain strain conditions. This suggests that adopting the conventional design approach may over-estimate the undrained shear strength and CSR where a pair of design planes intersect into a boundary line, examples of which occur in design of support of excavation top-down systems for deep basements and access shafts. For α = 60°, sand specimens consolidated under the relatively greater 400 kPa pressure reached the Quasi Steady State (Phase Transformation, QSS PT) and Critical Stress Ratio (CSR) at relatively greater effective deviatory pressure. For these specimens, the control of b-ratio appears to be negligible at QSS; suggesting that latter shortfall in conventional design approaches would have a limited impact on deviatory load at the point of phase transformation (Figs 9c-d).

Findings here are generally in agreement with previous findings of Shibuya and Hight [48] and Shibuya et al. [49]. Studying the interactions between b-ratio and undrained shear response for medium loose

HRS sand, they varied the α between 0° and 90° and adopted three *b*-ratio values of 0.0, 0.5 and 1.0. They concluded that increasing intermediate principal stress (*b*-ratio) from 0 to 0.5 has no significant effect on sand's response, whereas larger *b*-ratio values lead to the formation of weaker, soften and more brittle undrained behaviour. Yoshimine et al. [47] presented similar set of results for loose angular Toyoura Sand (D_{50} = 0.17 mm, e_{min} = 0.597, e_{max} = 0.977). The earlier studies of Poulos [50] and Poulos et al. [51] suggest the independency of stress path from sand's inherent anisotropy at large strains and as sand approaches the ultimate steady state. This is not consistent with findings here: the USS appears to be generally inversely proportional with the direction of principal stress axes and intermediate principal stress ratio.

3.3 Steady State for Fibre-reinforced Sand

The random distribution of fibres through the loose sand medium and the governing undrained conditions are believed here to have allowed fibres rest along multi-directional planes during the course of shearing. Isotropic consolidation under high confining stresses (to a closer packing) ensures that this initial random distribution of fibres remains through subsequent shearing phase. Confinement level matters and is discussed in more details in Section 3.4.

Contribution of the fibres to shear strength and plastic behaviour of fibre-reinforced sands is generally complicated, particularly when the intrinsically anisotropic sand-fibre mediums are subjected to anisotropic loading. Unreinforced and reinforced sand specimens were remoulded to a high initial void ratio in the range of 0.795 to 0.800. The stress-strain response of composite materials (i.e. sand reinforced with 1.5% fibre) is illustrated in Fig. 10.

Base sand shows a dilative response upon anisotropic shearing under relatively low α values (Figs. 9e, 9i, 9g and 9k). The dilative behaviour changes into a contractive strain softening response as α increases to 60° (Figs. 9a, 9c). Upon reinforcement with fibres, the dilative behaviour continues to be dominant at high α levels (Figs. 10a, 10c).

Figs. 10d, 10h and 10i demonstrate the difference between the t_{PT} in base and reinforced sand specimens (Δt_{PT}), where t_{PT} is t at phase transformation. At b = 0.5 (almost full compression, plain strain), Δt_{PT} sharply decrease with an increase in α from 15° to 30°. This suggests that in a compressive environment and plain strain conditions, torsional stresses decrease the contribution of fibres to undrained strength enhancement. The strain softening for base sand as P' reaches the phase transformation leads to a CSS state (Fig. 9d). At b=1 (counterbalancing extension), Δt_{PT} show marginal improvements with a rise in α from 15° to 30°, followed by substantial improvements as α grows to 60°. For when compressive stresses are counterbalanced with extension, torsional stresses appear to fully mobilise the tensile capacity of fibre inclusions, thereby a remarkable increase in the contribution of fibres to undrained strength enhancement takes place. This is an important new finding with many practical implications: The use of fibre-reinforced sands as subgrade for shallow footings or reinforced earth slopes is generally beneficial unless the system is expected to carry anisotropic loading. The composite system however appears to be useful as shallow subgrades housing a system of short micro-piles, underpinning a superstructure that applies transient loading or is expected to bear dynamic excitations.

Figure 11a illustrates the variation of Δq_{USS} (the difference of deviatoric stress at ultimate steady state USS between the reinforced and base sand at a reference deviatoric strain of 10%) with the principal stress direction, α. Fibres become more effective as principal stress direction increase. When torsional stresses combine with extension (b = 1), composite materials make the most benefit from the fibre inclusions to attain their maximum possible undrained strength.

Figs. 11b and 11c illustrate the variation of anisotropy ratio (AR) with inclination angle α, where AR is the maximum deviator stress divided by deviator stress at 10% strain at α = 60° (maximum torsion), as a measure of scale. In this, AR here is a measure of undrained strength for a range of loading scenarios (of varied level of loading anisotropy) with respect to the strength under maximum testing torsion. For sand-fibre composites, the variation of undrained strength with α (a measure of torsion) is little when

the composite system is sheared under conditions at which the compressive actions are partially counterbalanced with imposed extension. Fibres begin, even early stages of torsion (small α values), to mobilise upon extension and reach deviatory stresses close to the maximum attainable under full torsion. This lends further evidence to the significance of intrinsic anisotropy in reinforced sands. Therefore, fibre reinforcement decrease the unwelcomed anisotropy in samples which is desirable. *AR* at low α values and for sand-fibre composites gain lower values under high 400 kPa isotropic confining pressure. Examining this finding in conjunction with the established significance of inherent anisotropy, it appears that isotropic consolidation under higher confining stresses (to a closer packing) ensures that the initial randomly-distributed fibre layout continues over the shearing phase. The undrained strength and plastic behaviour of fibre-reinforced sand is dependent on system's inherent anisotropy.

3.4 Fibre Shape and Assembly Packing Quality

Findings here build on recent findings reported in Mandolini et al. [23]. The undrained shear strength and plastic behaviour of fibre-sand composites is fundamentally controlled by anisotropy. Mandolini et al. [23] used standard European Houston RF S28 siliceous angular to sub-angular sand (D_{50}=0.32 mm, C_u=1.70, C_c=1.1, G_s=2.65, e_{min}=1.000, e_{max}=0.630) together with 0.5% polypropylene fibres and conducted a series of CD torsional triaxial tests (b = 0, 0.07, 0.25, 0.50, 0.75, 1.00; α = 0°, 15°, 30°, 45°, 60°, 90°). In contrast with findings of this work, Mandolini et al. [23] presented experimental evidence for inverse relationship between the principal stress direction inclination and drained shear strength in fibre-reinforced sands. Assuming that the slightly different fibre content in the two studies has minimal effect, there appears to be links between confinement-induced 'self-organisation' of fibres and initial packing state; thereby a consensus on the implications of initial packing state is needed to be reached. A high 0.931-0.956 void ratio (post isotropic consolidation) was adopted [23], inferring a very loose initial state. These are higher, by and large, than the post isotropic consolidation void ratios achieved in the present work (0.795-0.800). Upon application of anisotropic stresses to loose assemblies of particles (sand grains mixed with highly eccentric rod-shape fibres), the fibres begin to adopt a vertical

orientation and gradually align with vertical walls of sand particles. This structural evolution disturbs the multidirectional alignment of fibres; fibres move relative to one another and take a parallel and vertical orientation. This arrangement forms a suite of internal weakness planes (laminated structures). This limits the potential benefits of soil inherent anisotropy under torsion as fibres only partially fall in extension, restricting the soil's mobilised tensile resistance. Findings are consistent with earlier discussions in Gray and Ohashi [10] where a direct relationship was established between inclinations of principal stresses and shear strength for dense reinforced sand.

3.5 Dimensionless State Indices

Two state index parameters are proposed. Flow potential, u_f is defined as a measure of flow (strain softening) and formulated in Equation 8 (see Yoshimine and Ishihara [46]). Flow potential is controlled by stress conditions in sand during both initial and shearing stages, so too the intermediate principal stress and direction of principal stresses. In Equation 8, P'_{PT} is the mean effective pressure at the point of phase transformation and P'_c is the mean isotropic confining pressure.

$$u_f = 1 - P'_{PT}/P'_c \tag{8}$$

Peak strength index, q_{peak}/P'_c, is effectively normalised peak undrained shear strength with confining pressure as measure of scale.

In Figs 12a and b, the dimensionless u_f is plotted against the angle of principal stress orientation. Strain softening is less pronounced when test soils are subjected to a degree of extension upon increasing *b*-ratio. When reinforced (with fibres), strain softening fully disappear in such torsional extension loading environment. Findings here are in agreement with earlier discussions. Figs 12c-d shows the variation of the peak strength index with principal stress inclination angle. For reinforced sand, the normalised strength sharply decrease under moderate torsional efforts (α = 30°), irrespective of the balance between applied compressive-tensile stresses. Reinforced soil systems are likely to experience

instability as torsional stresses increase; implying that maximum torsion is not necessarily a worst-case scenario in design.

4. Conclusions

Contribution of the fibres to shear strength and plastic behaviour of fibre-reinforced sands is generally complicated, particularly when the intrinsically anisotropic sand-fibre mediums are subjected to anisotropic loading. This study aimed to use the orientation of principal stress and soil initial packing state combined as a proxy parameter to explore and explain the plastic behaviour of fibre-reinforced sands. Observations suggest that:

1. Loose sand exhibits a dilative response upon anisotropic shearing under relatively low α values. The dilative behaviour changes into contractive strain softening as α increases to 60°.
2. Sand rapidly develops a strain softening response as *b*-ratio increases; such conditions take place when soil fall under combined extension and torsion. Under such circumstances, flow upon shearing appears to be most pronounced in sands under low confining pressures.
3. Upon reinforcement with fibres, the dilative behaviour at high α values continues to be dominant: In a compressive environment and plain strain conditions, torsional stresses lower the contribution of fibres to undrained strength enhancement. For when compressive stresses are counterbalanced with extension, torsional stresses appear to fully mobilise the tensile capacity of fibre inclusions and improving their contribution to undrained strength.
4. Fibres become more effective as principal stress direction increase. When torsional stresses are combined with extension ($b = 1$), composite materials make the most benefit from presence of fibres and attain maximum possible undrained strength.
5. Strain softening is generally less pronounced when soils are subjected to a degree of extension (increasing *b*-ratio). When sand is reinforced (with fibres), strain softening fully disappears in torsional extension loading environment.

6. Reinforced soil systems are likely to experience instability as torsional stresses increase; implying that maximum torsion is not necessarily a worst-case scenario in design.

5. References

1. Ishihara K, Acacio A, and Towhata I (1993) Liquefaction-induced ground damage in Dagupan in the July 16, 1990 Luzon earthquake. Soils and Foundations 33(1):133-154.

2. Chian SC, Tokimatsu K, Madabhushi SPG (2014) Soil liquefaction-induced uplift of underground structures: physical and numerical modeling. Journal of Geotechnical and Geoenvironmental Engineering 140:04014057:1-18

3. Ardeshiri-Lajimi S, Yazdani M, and Assadi-Langroudi, A (2016) A study on the liquefaction risk in seismic design of foundations. Geomechanics and Engineering 11(6):805-820.

4. Sabbar AS, Chegenizadeh A, and Nikraz H (2017) Static liquefaction of very loose sand-slag-bentonite mixtures. Soils and Foundations 57:341-356.

5. Yang J and Wei L (2012) Collapse of loose sand with the addition of fines: the role of particle shape. Geotechnique 62(12):1111-1125.

6. Hight DW, Bennell JD, Chana B, Davis PD, Jardine RJ and Porovi E (1997) Wave velocity and stiffness measurements of the Crag and Lower London Tertiaries at Sizewell. Geotechnique 47(3):451-474.

7. Jefferies MG, and Been K (2006) Soil liquefaction: A critical state approach, Taylor and Francis, Abingdon.

8. Arthur JRF, Chua KS, Dunstan T, and Rodriguez CJI (1980). Principal stress rotation: a missing parameter, Journal of Geotechnical Engineering Division ASCE 106(4):419-433.

9. Waldron LJ (1977) The shear resistance of root-permeated homogeneous and stratified soil. Soil Science Society of America Journal 41(5):843–849.

10. Gray DH, and Ohashi H (1983) Mechanics of fiber reinforcement in sand. Journal of Geotechnical Engineering ASCE 109:335–353.

11. Maher MH, and Gray DH (1990) Static response of sands reinforced with randomly distributed fibers. Journal of Geotechnical Engineering ASCE 116(11):1661-1677.

12. Michalowski RL, and Zhao A (1996) Failure of fiber-reinforced granular soils. Journal of Geotechnical Engineering ASCE 122(3):226-234.

13. Michalowski RL, and Cermák J (2003) Triaxial compression of sand reinforced with fibers. Journal of Geotechnical and Geoenvironmental Engineering ASCE 129(2):125-136.

14. Michalowski RL (2008) Limit analysis with anisotropic fibre-reinforced soil. Geotechnique. 58(6):489–501.

15. Diambra A, Russell AR, Ibraim E, Wood DM (2007) Determination of fibre orientation distribution in reinforced sands. Geotechnique 57(7):623–628.

16. Ibraim E, Diambra A, Russell AR, Wood DM (2012) Assessment of laboratory sample preparation for fibre reinforced sands. Geotextile and Geomembranes 34:69–79.

17. Jewell RA, Wroth CP (1987) direct shear tests on reinforced sand. Geotechnique 37(1):53–68.

18. Palmeira EM and Milligan WE (1989) Scale and other factors affecting the results of pull-out tests of grids buried in sand. Geotechnique 39:511-24.

19. Symes MJ (1983) Rotation of principal stresses in sand. Imperial College of Science, London, UK.

20. Sayão A and Vaid Y (1996) Effect of intermediate principal stress on the deformation response of sand. Canadian Geotechnical Journal 33:822-828.

21. Li C (2005) Mechanical Response of Fiber-Reinforced Soil. the University of Texas at Austin, USA.

22. Diambra A, Ibraim E, Wood DM, Russell AR (2010) Fibre reinforced sands: experiments and modelling. Geotextiles and Geomembranes 28(3):238–250.

23. Mandolini A, Diambra A, and Ibraim E (2019) Strength anisotropy of fibre reinforced sands under multiaxial loading. Geotechnique 69(3):203-216.

24. Shibuya S (1985). Undrained behaviour of granular materials under principal stress rotation. Imperial College of Science, London, UK.

25. Menkiti CO (1995) Behaviour of clay and clayey-sand, with particular reference to principal stress rotation. Imperial College of Science, London, UK.

26. Zdravkovic L (1996) The stress-strain-strength anisotropy of a granular medium under general stress conditions. Imperial College of Science, London, UK.

27. Porovic, E (1995). Investigations of soil behaviour using a resonant column torsional shear hollow cylinder apparatus. Imperial College of Science, London, UK.

28. Jardine RJ and Menkiti CO (1999) The undrained anisotropy of K_0 consolidated sediments. In: Proceedings of the 12th ECSMFE Geotechnical engineering for transportation infrastructure, Rotterdam, 1101-1108.

29. Jardine RJ, Zdravkovic L, Porovic E (1997) Anisotropic Consolidation Including Principal Stress Axis Rotation: Experiments, Results and Practical Implications, XIVth ICSMFE, Hamburg. 2165-2169.

30. Yoshimine M, Ishihara K and Vargas W (1998) Flow deformation of sands subjected to principal stress rotation. Soils and Foundations 38(3): 179–188.

31. Symes MJ, Gens A and Hight DW (1985). Discussion: The development of a new hollow cylinder apparatus for investigating the effects of principal stress rotation in soils undrained anisotropy and principal stress rotation in saturated sand. Géotechnique 35(1):78-85.

32. Nakata Y, Hyodo M, Murata H and Yasufuku N (1998) Flow deformation of sands subjected to principal stress rotation. Soils and Foundations 38(2):115-128.

33. Vaid YP, Sivathayalan S, Uthayakumar M and Eliadorani A (1995) Liquefaction potential of reconstituted Syncrude sand. In: Proceedings of the 48th Canadian Geotechnical Conference, Vancouver, Canada: 319-328.

34. Vaid YP, Uthayakumar M, Sivathayalan S, Robertson PK and Hofman B (1995) Laboratory testing of Syncrude Sand. In: Proceedings of the 48th Canadian Geotechnical Conference, Vancouver, Canada: 223-232.

35. Uthayakumar M and Vaid YP (1998) Static liquefaction of sands under multiaxial loading. Canadian Geotechnical Journal 35: 273-283.

36. Diambra A and Ibraim E (2015) Fibre-reinforced sand: interaction at the fibre and grain scale. Géotechnique 64(4):296-308.

37. Shukla SK (2017) Fundamentals of Fibre-Reinforced Soil Engineering. Springer.

38. Consoli NC, Casagrande MDT and Coop MR (2005) Effect of fibre reinforcement on the isotropic compression behaviour of a sand. Journal of Geotechnical and Geoenvironmental Engineering 131:1434-1436.

39. Soriano I, Ibraim E, Ando E, Diambra A, Laurencin T, Moro P, and Viggiani G (2017) 3D fibre architecture of fibre-reinforced sand. Granular Matter 19(4):75.

40. Mirzababaei M, Arulrajah A, Haque A, Nimbalkar S, and Mohajerani A (2018) Geosynthetics International 25(4):471-480.

41. Marri A, Uddin S and Wanatowski D (2014) Sample preparation technique for fibre reinforced cemented soils. Procedia Engineering 77:140-147.

42. Ibraim E and Fourmont S (2006) Behaviour of sand reinforced with fibres. In: Proceedings of the geotechnical symposium, geomechanics: laboratory testing, modelling and applications, Rome, Italy. Eds. Ling HI, Callisto L, Leshchinsky D and Koseki J: 807-818.

43. Lade, PV and Ibsen LB (1997) A study of the phase transformation and the characteristic lines of sand behaviour. International Symposium on Deformation and Progressive Failure in Geomechanics, Nagoya, Japan.

44. Robertson PK, Wride CE, List BR, Atukorala U, Biggar KW, Byrne PM, Campanella RG, Cathro DC, Chan DH, Czajewski K, Finn WDL, Gu WH, Hammamji Y, Hofmann BA, Howie JA, Hughes J, Imrie AS, Konrad JM, Kupper A, Law T, Lord ER, Monahan PA, Morgenstern NR, Philips R, Piche R, Plewses HD, Scott D, Sego DC, Sobkowicz J, Stewart RA, Watts BD, Woeller DJ, Youd TL, and Zavodni Z (2000) The CANLEX project: summary and conclusions. Canadian Geotechnical Journal 37(3):563-591.

45. Vaid YP, Sivathayalan S (2000) Fundamental factors affecting liquefaction susceptibility of sands. Canadian Geotechnical Journal 37:592–606.

46. Yoshimine M and Ishihara K (1998) Flow potential of sands during liquefaction. Soils and Foundations 38(3):189-198.

47. Yoshimine M, Robertson PK and Wride CE (1999) Undrained shear strength of clean sands to trigger flow liquefaction. Canadian Geotechnical Journal 36:891-906.

48. Shibuya S and Hight DW (1987) Patterns of cyclic principal stress rotation and liquefaction. In: Proceedings of the 8th Asian Regional Conference on Soil Mechanics and Foundation Engineering, Kyoto, Japan, 1:265-268.

49. Shibuya S, Hight DW and Jardine RJ (2003) Local boundary surface of a loose sand dependent on consolidation path. Soils and Foundations (43)3:85-93.

50. Poulos SJ (1981) the steady state of deformation. Journal of Geotechnical Engineering ASCE 107:553-562.

51. Poulos SJ, Castro G and France JW (1985) Liquefaction evaluation procedure. Journal of Geotechnical Engineering ASCE 111(6):772-792.

52. ASTM D6913 / D6913M-17 Standard test methods for particle size distribution (gradation) of soils using sieve analysis, ASTM International, West Conshohocken, PA.

53. ASTM D854-14 (2014) Standard test methods for specific gravity of soil solids by water pycnometer, ASTM International, West Conshohocken, PA.

54. ASTM D4254-16 (2016) Standard test methods for minimum index density and unit weight of soils and calculation of relative density, ASTM International, West Conshohocken, PA.

55. ASTM D4253-16 (2016) Standard test methods for maximum index density and unit weight of soils using a vibratory table, ASTM International, West Conshohocken, PA.

List of Figures

Fig. 1 (a) Particle size distribution, (b) Sub-angular shape of F161 Sand component in SEM micrographs

Fig. 2 Fibres used in this study in image

Fig. 3 (a) Sand-fibre mixture specimen, (b) Fibre orientation in sand-fibre specimen, (c) Sand-fibre during the mixing phase

Fig. 4 (a) Schematic diagram of Hollow Cylinder Torsional Shear (HCTS) apparatus, (b) A specimen under test in HCTS chamber

Fig. 5 The α° and b-value in stress space

Fig. 6 Stress state in the wall of HCTS specimen during torsion shear test

Fig. 7 A typical HCTS specimen before and after testing

Fig. 8 Stress path and stress-strain response of sand during undrained shearing: (a) typical stress path, phase transformation and steady states, (b) stress path and stress-strain behaviour in sands of varied packing states

Fig. 9 Steady States for base sand under inclined deviatory load and varying b-ratio (USS = ultimate steady state; ESP =effective stress path; TSP = total stress path; CSS = critical steady state; CSR = critical stress ratio; QSS = quasi steady state), (a)-(e)-(i): stress-strain under P'=200 kPa and for varying α; (c)-(g)-(k): stress-strain under P'=400 kPa and for varying α; (b)-(f)-(j): stress path under P'=200 kPa and for varying α; (d)-(h)-(l): stress path under P'=400 kPa and for varying α

Fig. 10 Steady States for base and reinforced sand under inclined deviatory load and varying b-ratio (USS = ultimate steady state; ESP =effective stress path; TSP = total stress path; CSS = critical steady state; CSR = critical stress ratio; QSS = quasi steady state), (a)-(e)-(i): stress-strain under P'=200 kPa and for varying α; (c)-(g)-(k): stress-strain under P'=400 kPa and for varying α; (b)-(f)-(j): stress path under P'=200 kPa and for varying α; (d)-(h)-(l): stress path under P'=400 kPa and for varying α

Fig. 11 Effect of α on undrained shear strength of base and reinforced sands: (a) improvement in USS upon reinforcement as a function of α and b, (b-c) normalised deviatory stress at USS as a measure of dependency of undrained shear strength on α

Fig. 12 Effect of α on dimensionless state indices

List of Tables

Table 1 Geometrical and physico-mechanical properties of materials

Table 2 List of the torsional CU tests conducted on base sand and reinforced sand using the HCTA

Table 1

Material	Property	Value	Unit	Measurement methods
Sand	Grain diameter at 10% passing (D_{10})	132.3	µm	ASTM D6913 [52]
	Grain diameter at 50% passing (D_{50})	235.3	µm	ASTM D6913 [52]
	Grain diameter at 90% passing (D_{90})	437.7	µm	ASTM D6913 [52]
	Coefficient of uniformity (C_u)	0.97	-	ASTM D6913 [52]
	Coefficient of curvature (C_C)	1.78	-	ASTM D6913 [52]
	Specific gravity (G_s)	2.68	-	ASTM D854 [53]
	Minimum void ratio (e_{min})	0.548	-	ASTM D4254 – 16 [54]
	Maximum void ratio (e_{max})	0.874	-	ASTM D4253 – 16 [55]
	Roundness ratio R	0.42	-	
	Sphericity ratio S	0.60	-	
	Fines content (FC) %	0.00	-	ASTM D6913 [52]
Fibre	Fibre length (l_f)	15.0	mm	
	Fibre diameter (D_f)	0.2	mm	
	Fibre aspect ratio (AR_F)	55.55	-	
	Young's modulus (E)	3.6	GPa	Provided by supplier
	Tensile resistance (T_y)	450	MPa	Provided by supplier

Table 2

Test No.	Loading type	w_f (%) †	P'_c (kPa)	α (º)	b	e_c^*
H200f0-0.5-15	Compression	0.0	200	15	0.5	0.793
H200f0-0.5-30	Compression + Torsion	0.0	200	30	0.5	0.794
H200f0-0.5-60	Torsion	0.0	200	60	0.5	0.800
H200f0-1-15	Compression	0.0	200	15	1.0	0.797
H200f0-1-30	Compression + Torsion	0.0	200	30	1.0	0.796
H200f0-1-60	Torsion	0.0	200	60	1.0	0.800
H200f1.5-0.5-15	Compression	1.5	200	15	0.5	0.795
H200f1.5-0.5-30	Compression + Torsion	1.5	200	30	0.5	0.796
H200f1.5-0.5-60	Torsion	1.5	200	60	0.5	0.799
H200f1.5-1-15	Compression	1.5	200	15	1.0	0.800
H200f1.5-1-30	Compression + Torsion	1.5	200	30	1.0	0.798
H200f1.5-1-60	Torsion	1.5	200	60	1.0	0.797
H400f0-0.5-15	Compression	0.0	400	15	0.5	0.800
H400f0-0.5-30	Compression + Torsion	0.0	400	30	0.5	0.798
H400f0-0.5-60	Torsion	0.0	400	60	0.5	0.795
H400f0-1-15	Compression	0.0	400	15	1.0	0.800
H400f0-1-30	Compression + Torsion	0.0	400	30	1.0	0.795
H400f0-1-60	Torsion	0.0	400	60	1.0	0.800
H400f1.5-0.5-15	Compression	1.5	400	15	0.5	0.796
H400f1.5-0.5-30	Compression + Torsion	1.5	400	30	0.5	0.797
H400f1.5-0.5-60	Torsion	1.5	400	60	0.5	0.796
H400f1.5-1-15	Compression	1.5	400	15	1.0	0.797
H400f1.5-1-30	Compression + Torsion	1.5	400	30	1.0	0.799
H400f1.5-1-60	Torsion	1.5	400	60	1.0	0.798

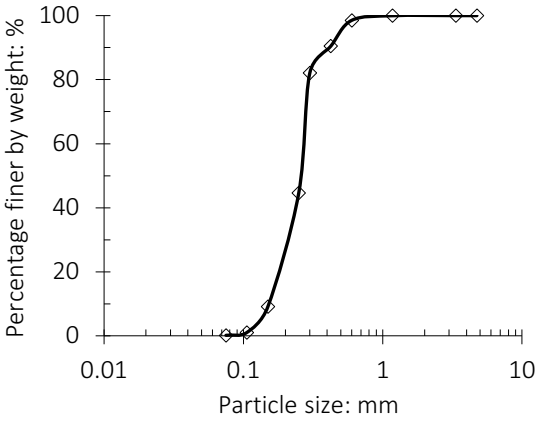
Percentage finer by weight: %
100
80
60
40
20
0
0.01
0.1
1
10
Particle size: mm

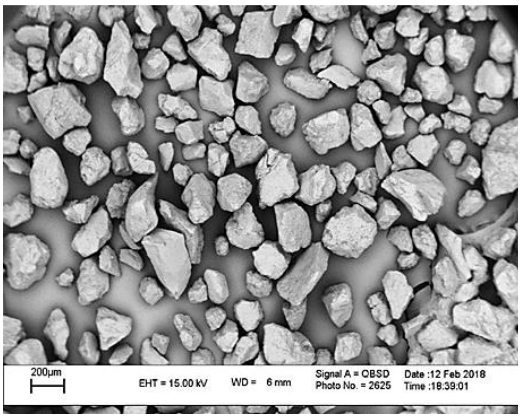
200µm
EHT = 15.00 kV
WD = 6 mm
Signal A = QBSD
Photo No. = 2625
Date :12 Feb 2018
Time :18:39:01

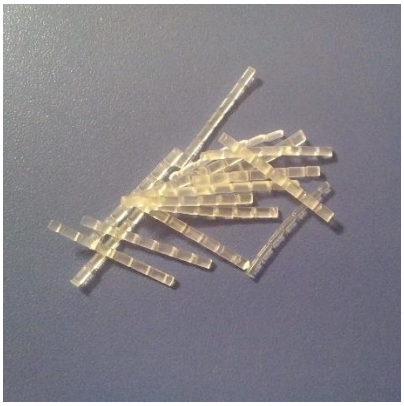

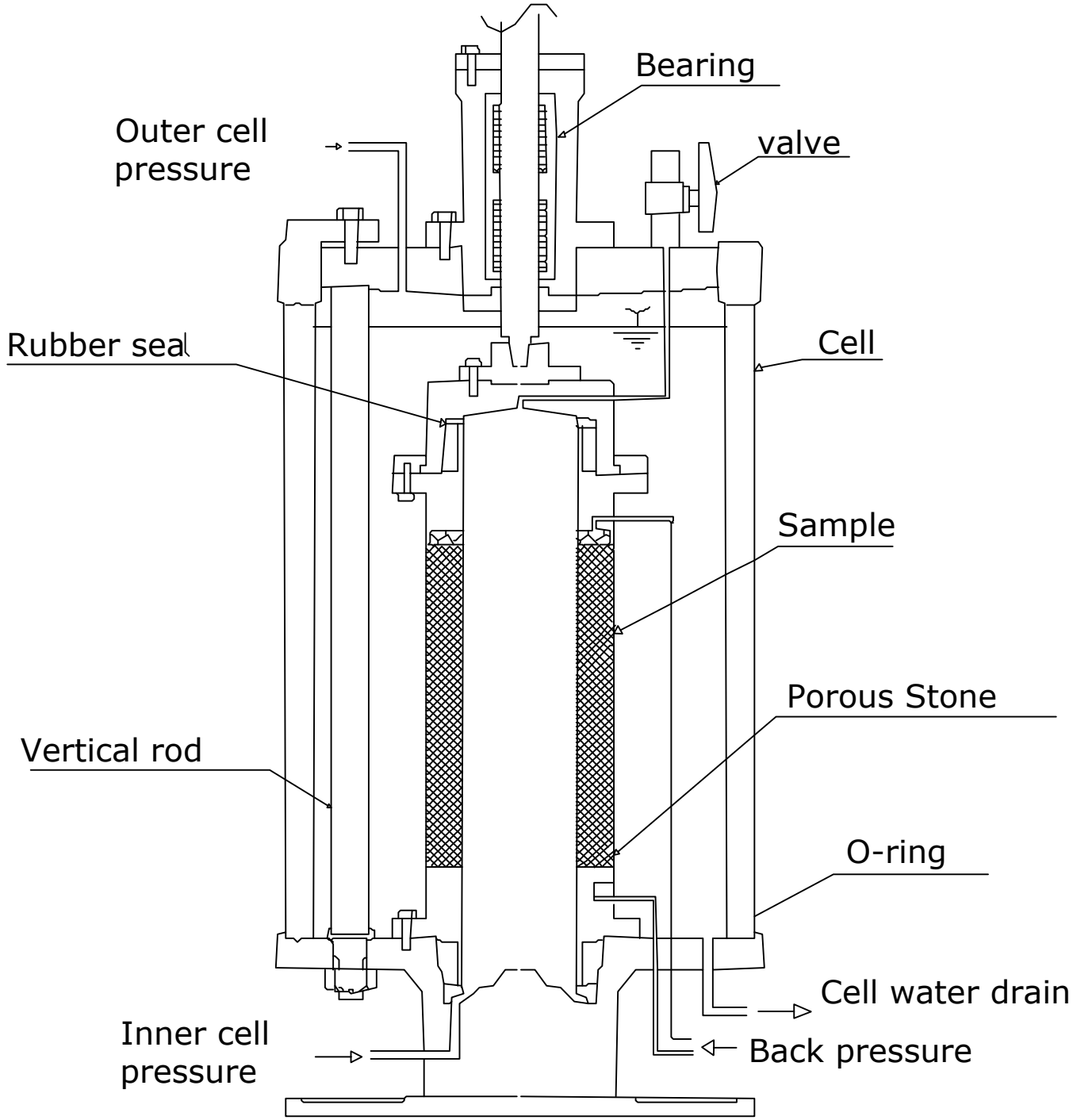
Bearing
Outer cell
pressure
valve
Rubber seal
Cell
Sample
Porous Stone
Vertical rod
O-ring
Cell water drain
Inner cell
pressure
Back pressure

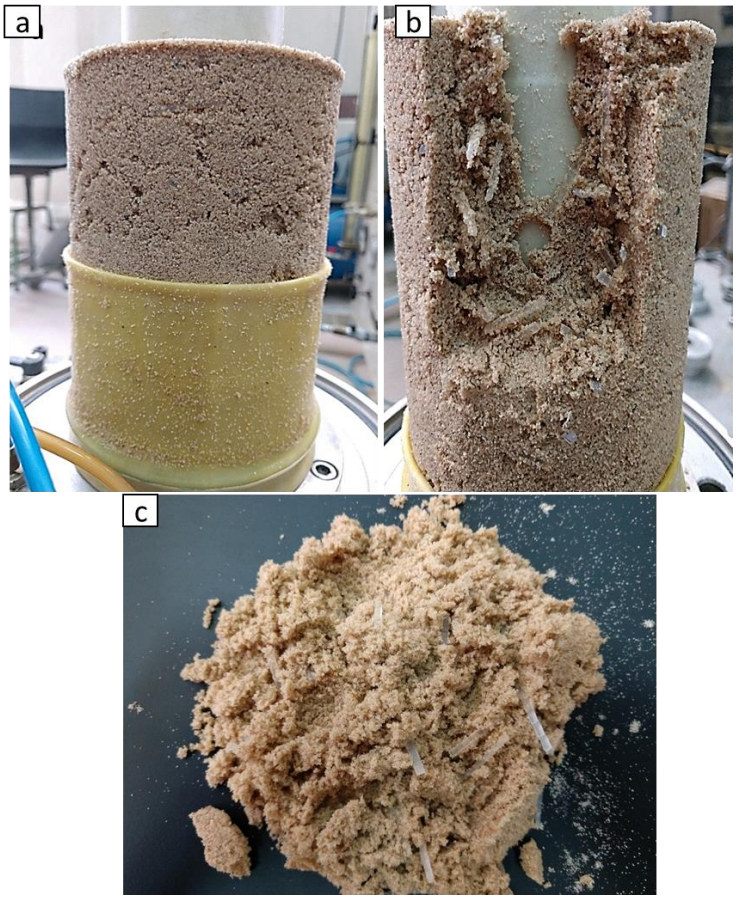
a
b
c

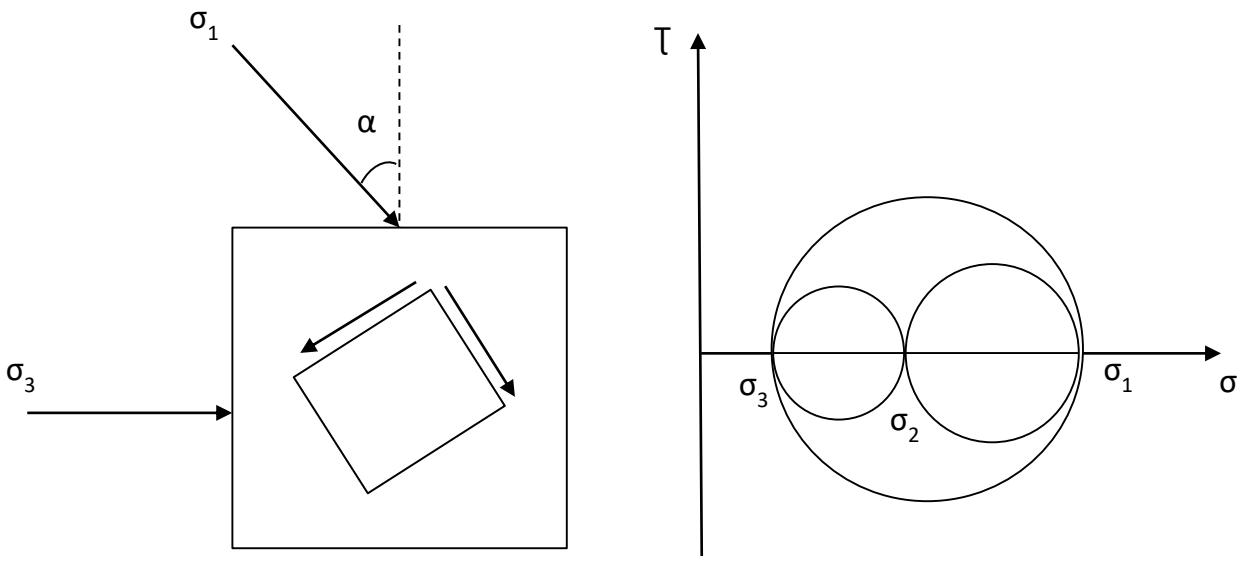
σ1
α
σ3
τ
σ3
σ2
σ1
σ

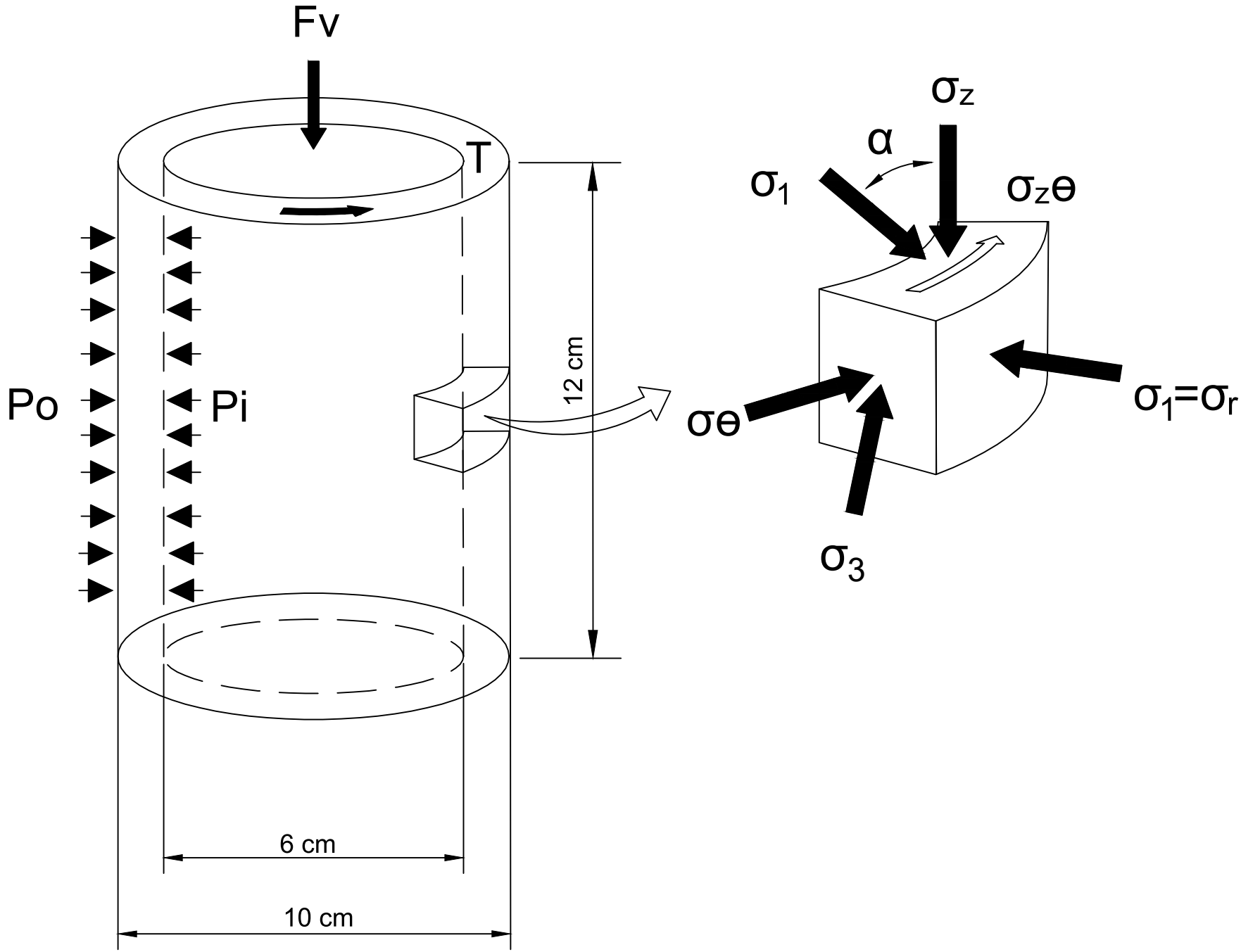
Fv
T
Po
Pi
12 cm
6 cm
10 cm
σz
α
σ1
σzθ
σθ
σ1=σr
σ3

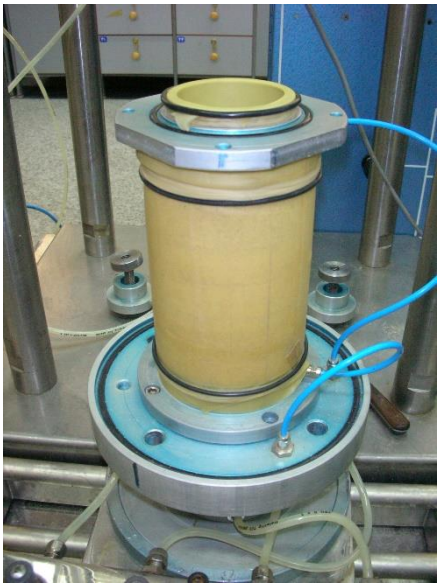

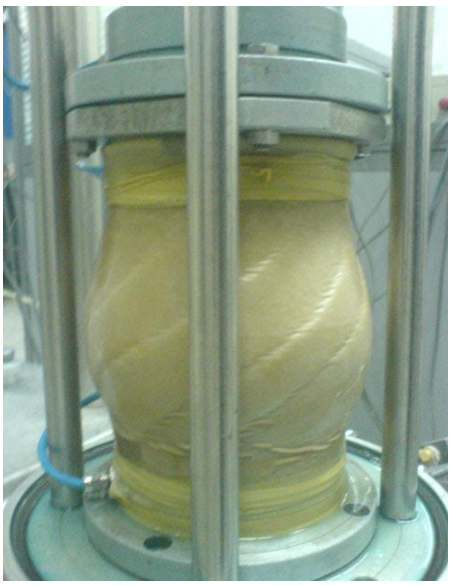

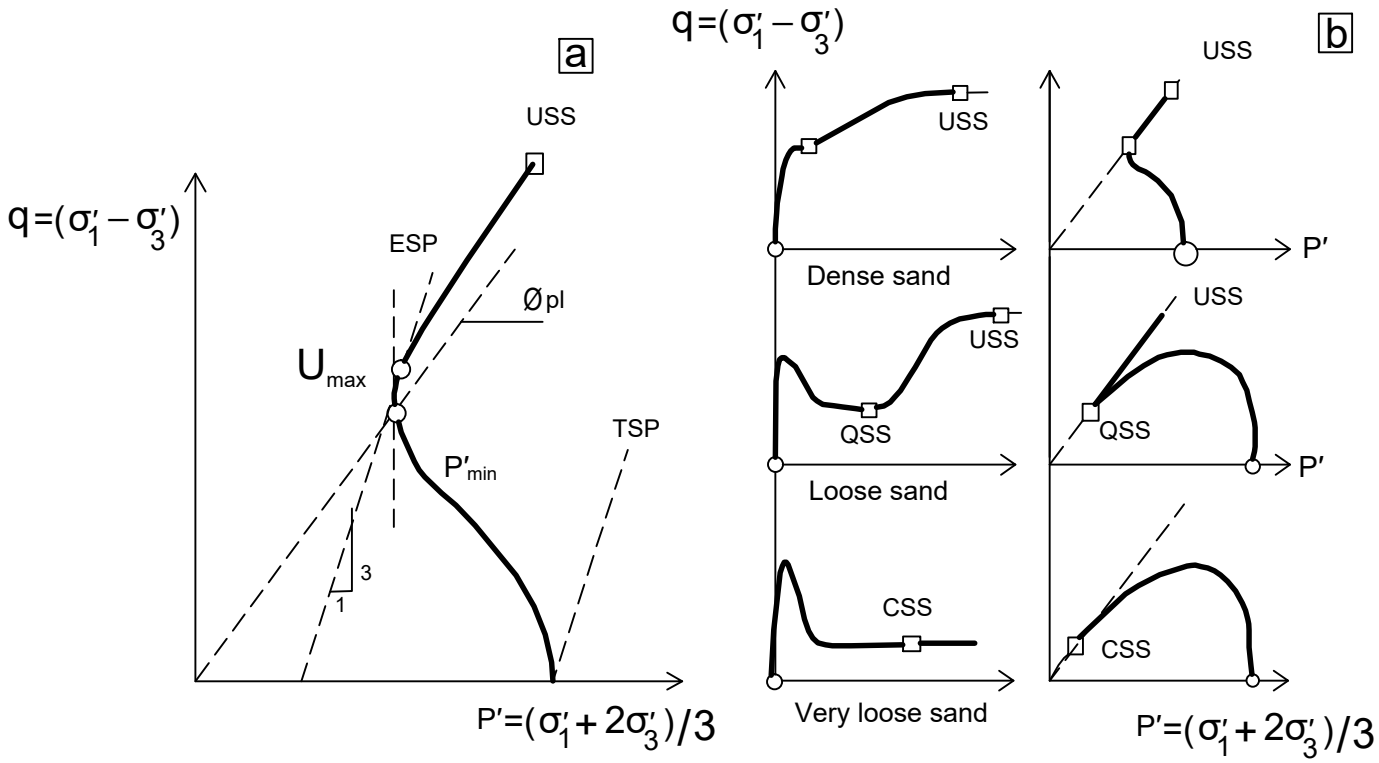
a
b
q=(σ′1 − σ′3)
USS
ESP
Øpl
Umax
P′min
TSP
3
1
P′=(σ′1 + 2σ′3)/3
Dense sand
Loose sand
Very loose sand
QSS
CSS
P′

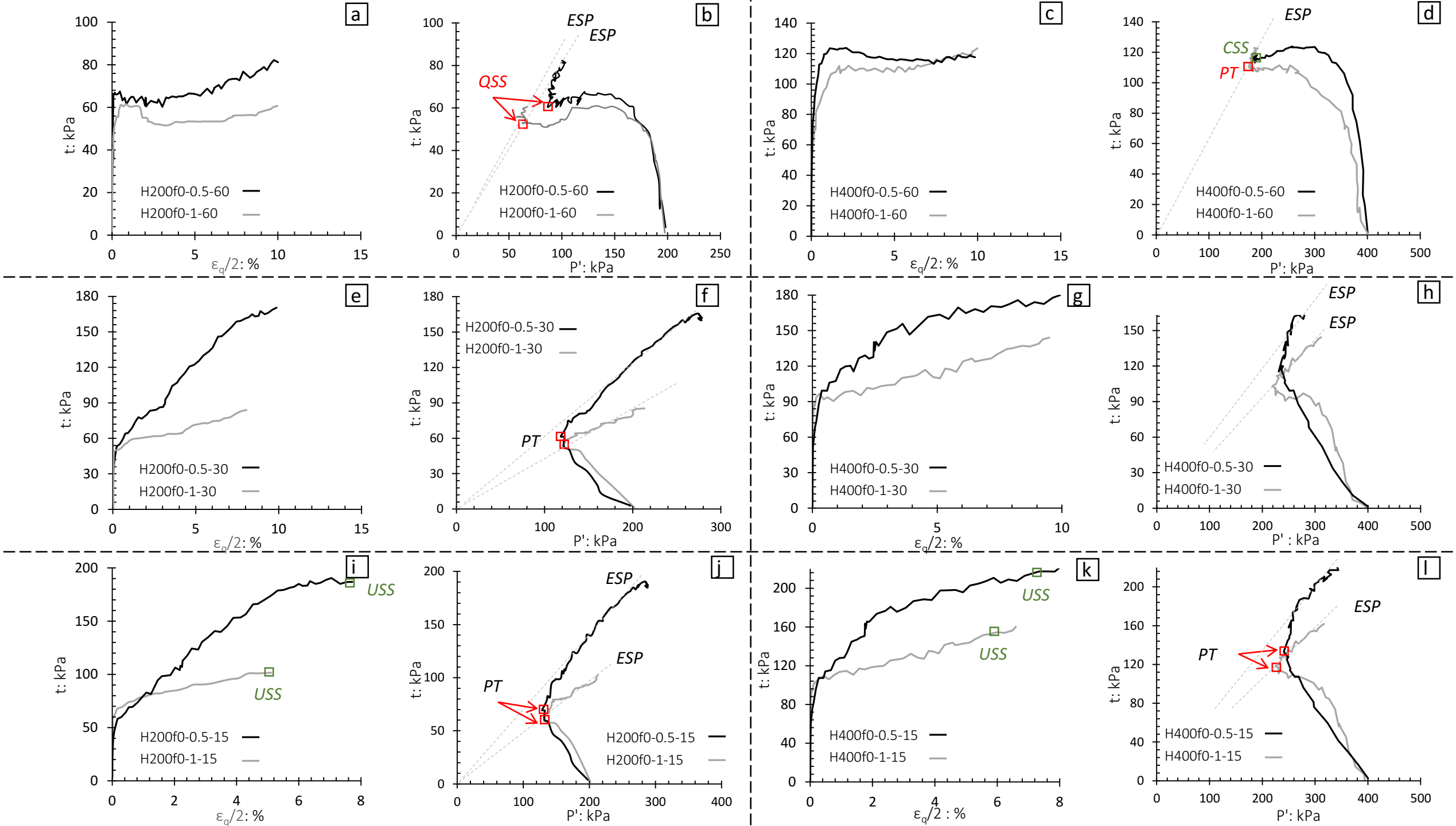
a
t: kPa
εq/2: %
H200f0-0.5-60
H200f0-1-60
b
ESP
ESP
QSS
P': kPa
H200f0-0.5-60
H200f0-1-60
c
H400f0-0.5-60
H400f0-1-60
d
ESP
CSS
PT
H400f0-0.5-60
H400f0-1-60
e
H200f0-0.5-30
H200f0-1-30
f
H200f0-0.5-30
H200f0-1-30
PT
g
H400f0-0.5-30
H400f0-1-30
h
ESP
ESP
H400f0-0.5-30
H400f0-1-30
i
USS
USS
H200f0-0.5-15
H200f0-1-15
j
ESP
ESP
PT
H200f0-0.5-15
H200f0-1-15
k
USS
USS
H400f0-0.5-15
H400f0-1-15
l
ESP
PT
H400f0-0.5-15
H400f0-1-15

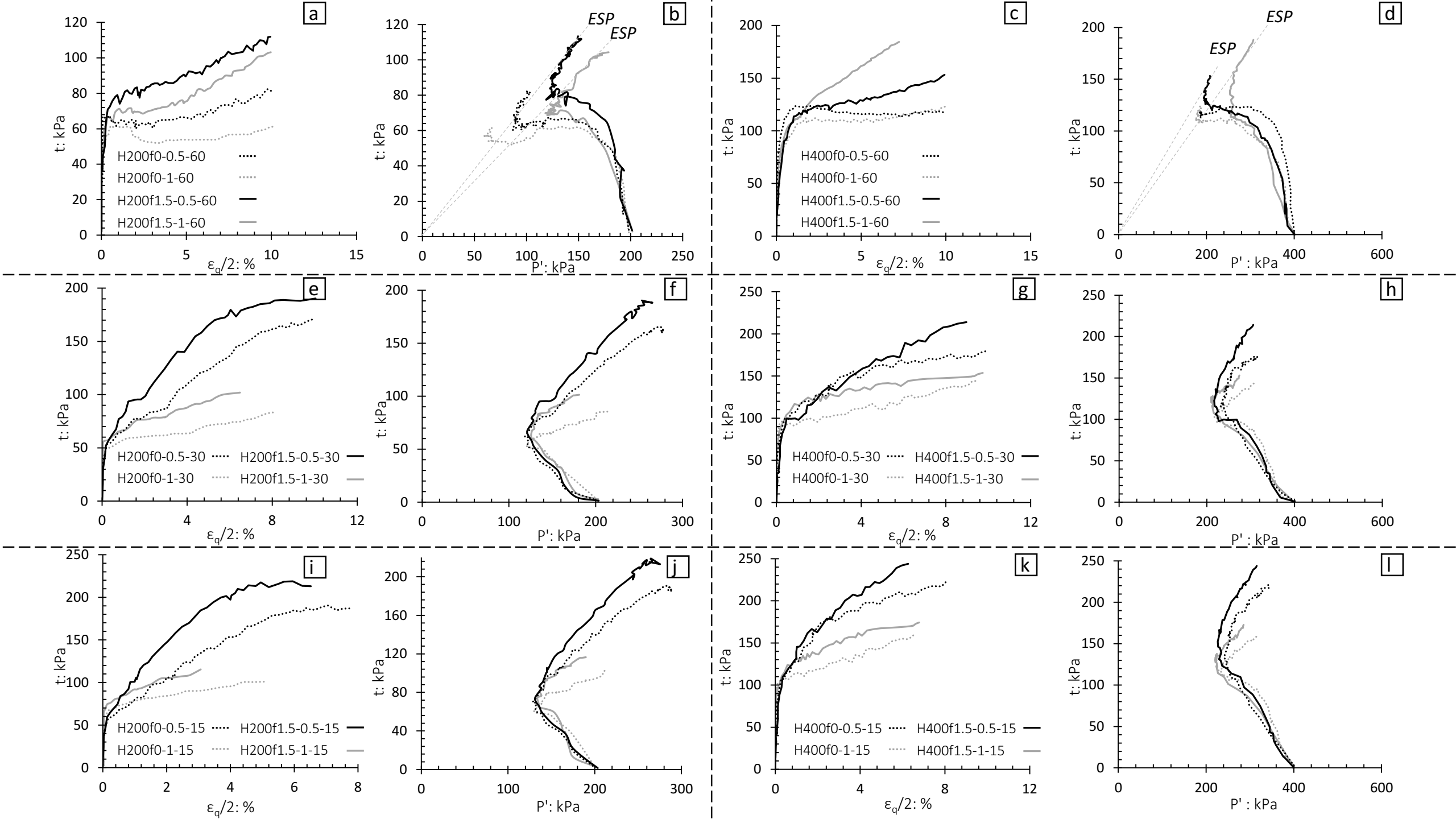
a
b
c
d
e
f
g
h
i
j
k
l
ESP
t: kPa
P': kPa
$\varepsilon_q/2$: %
H200f0-0.5-60
H200f0-1-60
H200f1.5-0.5-60
H200f1.5-1-60
H400f0-0.5-60
H400f0-1-60
H400f1.5-0.5-60
H400f1.5-1-60
H200f0-0.5-30
H200f0-1-30
H200f1.5-0.5-30
H200f1.5-1-30
H400f0-0.5-30
H400f0-1-30
H400f1.5-0.5-30
H400f1.5-1-30
H200f0-0.5-15
H200f0-1-15
H200f1.5-0.5-15
H200f1.5-1-15
H400f0-0.5-15
H400f0-1-15
H400f1.5-0.5-15
H400f1.5-1-15

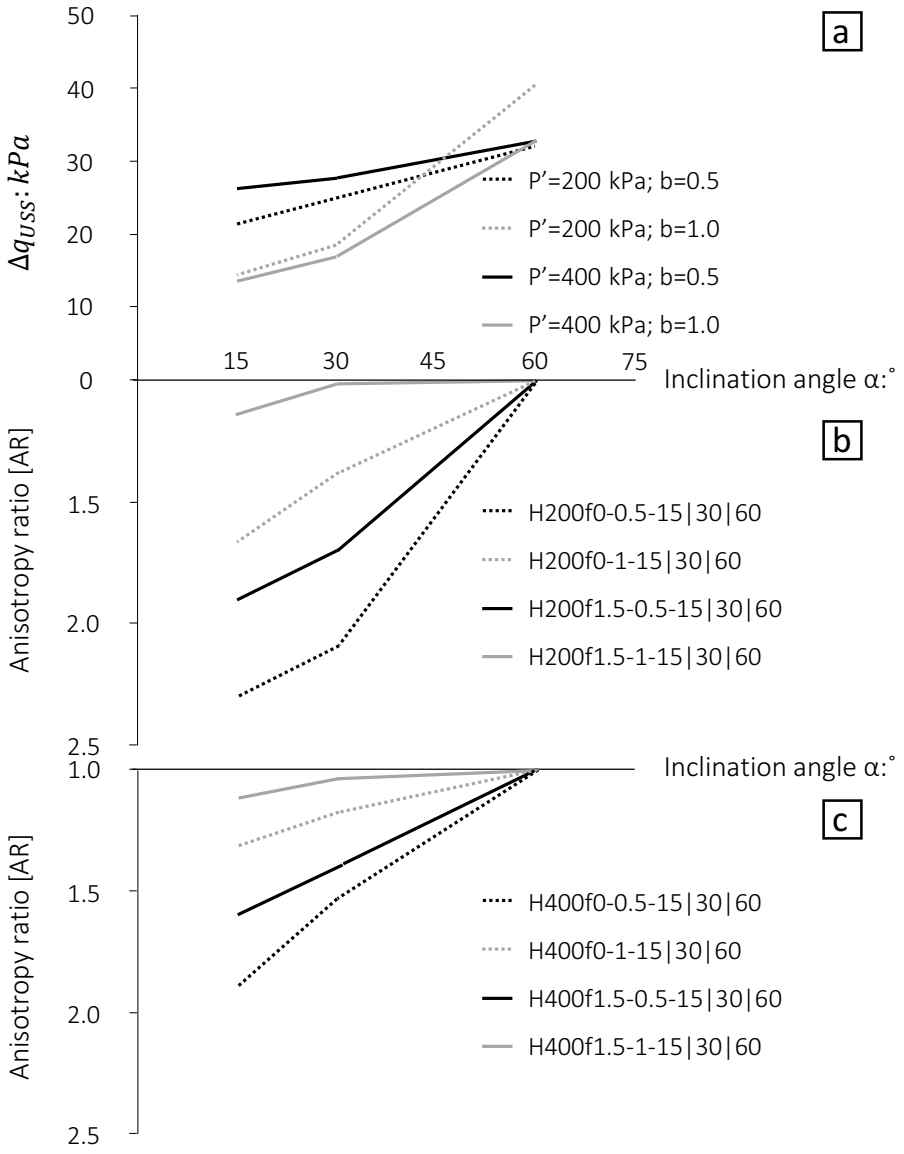
a
50
40
30
20
10
0
$\Delta q_{USS}: kPa$
P'=200 kPa; b=0.5
P'=200 kPa; b=1.0
P'=400 kPa; b=0.5
P'=400 kPa; b=1.0
15
30
45
60
75
Inclination angle α:˚
b
Anisotropy ratio [AR]
1.5
2.0
2.5
H200f0-0.5-15|30|60
H200f0-1-15|30|60
H200f1.5-0.5-15|30|60
H200f1.5-1-15|30|60
Inclination angle α:˚
c
1.0
1.5
2.0
2.5
Anisotropy ratio [AR]
H400f0-0.5-15|30|60
H400f0-1-15|30|60
H400f1.5-0.5-15|30|60
H400f1.5-1-15|30|60

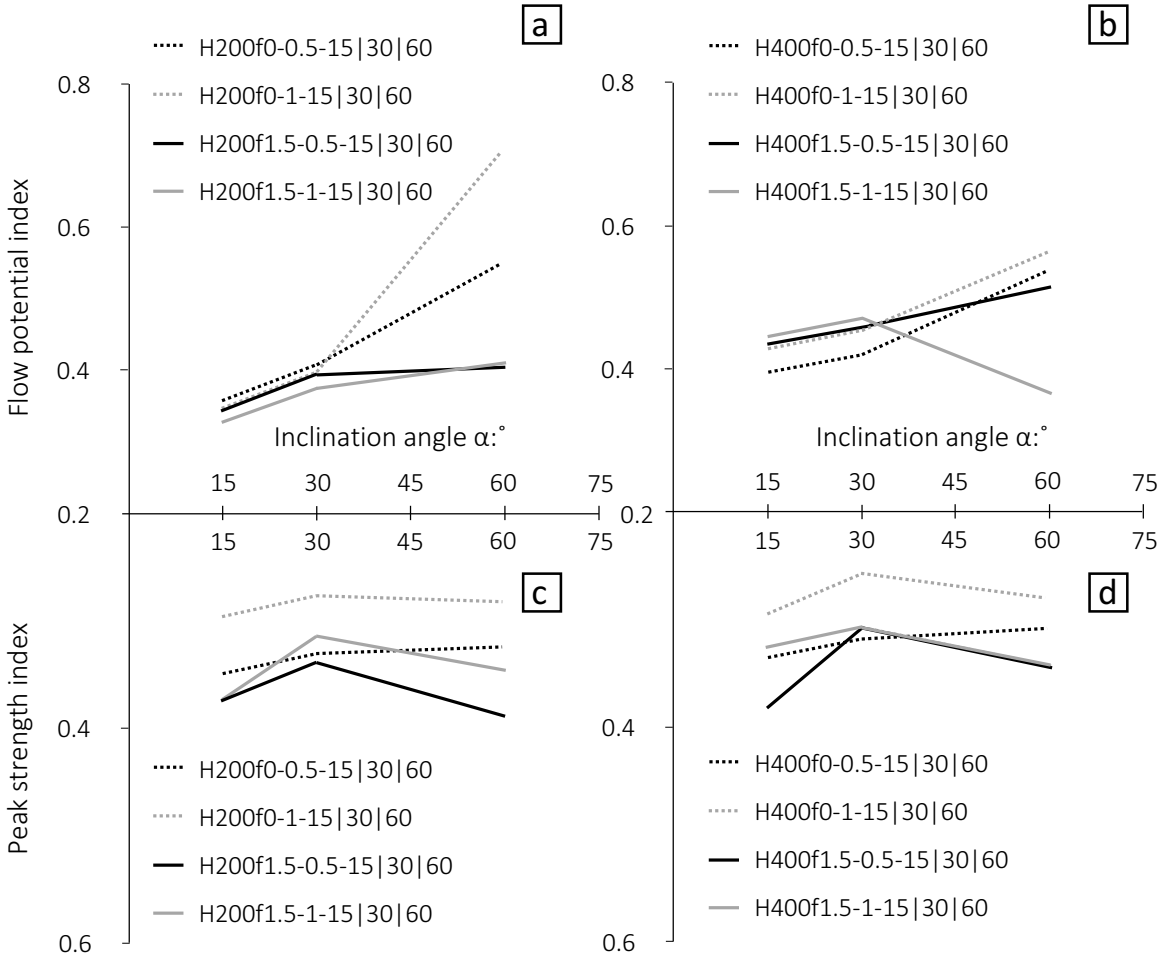
a
b
c
d
H200f0-0.5-15|30|60
H200f0-1-15|30|60
H200f1.5-0.5-15|30|60
H200f1.5-1-15|30|60
H400f0-0.5-15|30|60
H400f0-1-15|30|60
H400f1.5-0.5-15|30|60
H400f1.5-1-15|30|60
Flow potential index
Peak strength index
Inclination angle α:˚
0.8
0.6
0.4
0.2
15
30
45
60
75